# Surface functionalization of graphene oxide with poly(2-hydroxyethyl methacrylate)-*graft*-poly(ε-caprolactone) and its electrospun nanofibers with gelatin

**Bakhshali Massoumi**[1] · **Fereshteh Ghandomi**[1] · **Mojtaba Abbasian**[1] · **Morteza Eskandani**[2] · **Mehdi Jaymand**[2]

**Abstract** This article describes covalent functionalization of graphene oxide (GO) with poly(2-hydroxyethyl methacrylate)-*graft*-poly(ε-caprolactone) [P(HEMA-*g*-CL)] via 'living' polymerization techniques and preparation of its electrospun nanofibers with gelatin. For this purpose, the GO was synthesized by oxidizing pristine graphite powder and then acetyl chloride was incorporated into the GO to afford an atom transfer radical polymerization (ATRP) macroinitiator (GO-Cl). The synthesized macroinitiator was employed for HEMA polymerization via ATRP technique to produce GO-*g*-PHEMA. Afterward, CL was graft copolymerized from the hydroxyl groups of the PHEMA via ring-opening polymerization approach to afford GO-*g*-[P(HEMA-*g*-CL)] nanocomposite. The solutions of the GO-*g*-[P(HEMA-*g*-CL)] and gelatin were electrospun to fabricate uniform, conductive, and biocompatible nanofibers. The morphology, in vitro degradability, biocompatibility, hydrophilicity, and conductivity of the GO-*g*-[P(HEMA-*g*-CL)]/gelatin electrospun nanofibers were investigated. It is expected that the prepared nanofibers find application as a scaffolding biomaterial for regenerative medicine, mainly due to their biocompatibility, degradability, and electrical conductivity.

✉ Mehdi Jaymand
m_jaymand@yahoo.com; m.jaymand@gmail.com;
jaymandm@tbzmed.ac.ir

[1] Department of Chemistry, Payame Noor University,
P.O. Box 19395-3697, Tehran, Islamic Republic of Iran

[2] Research Center for Pharmaceutical Nanotechnology, Tabriz
University of Medical Sciences,
P.O. Box 51656-65811, Tabriz, Islamic Republic of Iran

## 1 Introduction

It is an unquestionable fact that graphene (G), a one-atom-thick hexagonal lattice of $sp^2$ carbon atoms, has attracted a great deal of interest on the basis of its importance in basic scientific research and potential applications including transparent conductors [1], (bio)chemical sensors [2], solar cells [3], nanoelectronic devices [4], nanocomposite (NC) materials, [5] as well as biomedical sciences [6, 7]. This tendency arises from its unique structural and physico-chemical characteristics that can be tuned through the manipulation of size, shape, and $sp^2/sp^3$ content, which make it as a promising material for a wide variety of applications [8–11]. The most commonly used approaches to obtain defect-free and high-quality graphene nanosheets are chemical vapor deposition and micromechanical cleavage of graphite [12, 13].

However, the low processability and strong interaction between individual graphene nanosheets are major drawbacks and restrict its application range in different fields. An efficient and versatile method to overcome these deficiencies is oxidation of graphite to graphene oxide (GO), subsequently modification of GO through reactive oxygen functional groups (e.g., epoxide, hydroxyl, and carboxyl groups) on its edge and basal planes to obtain novel multi-functional nanomaterials [14–17]. Thus, GO has good dispersibility in water, mainly due to its strong hydrophilicity. Nevertheless, the exfoliation of GO in common organic solvents is difficult, in part due to strong interlayer hydrogen bonds between mentioned oxygen functional groups [18, 19].

This problem can be circumvented through the functionalization of GO nanosheets with organic moieties; subsequently further stabilizing can be achieved by growth of polymer chains. There are two main strategies that can be employed for the grafting polymers to the surface of the

GO, which are defined as 'grafting to,' and 'grafting from' approaches [20–22]. The former method can be considered as in situ polymerization method, since grafting process is occurred by polymerization in the presence of different substrates. The 'grafting from' route requires immobilization initiators onto the GO surface followed by surface-initiated polymerization (SIP) and formation of a dense polymer brushes [23–25].

Among the various approaches for the 'grafting from' technique, reversible deactivation radical polymerization (RDRP; otherwise known as controlled or 'living' radical polymerization) methods including atom transfer radical polymerization (ATRP) [26, 27], nitroxide-mediated polymerization (NMP) [28, 29], and reversible addition of fragmentation chain transfer (RAFT) polymerization [30, 31] have stimulated great research efforts. Among them, the ATRP seems to be the most versatile and efficient methodology for the synthesis of well-defined, complex macromolecular architectures, as well as wide range of functionalities. In addition, in this approach, only negligible homopolymer is formed when employed in graft copolymerization [32–34].

In the category of the 'living' polymerization techniques, ring-opening polymerization (ROP) approach can be considered as a powerful approach to synthesize polymer brushes [35, 36]. This polymerization technique exhibits fast reaction kinetics under normal reaction conditions and has its own characteristics and advantages over other 'living' polymerization techniques. Most of the monomers of ROP are cyclic compounds such as lactides or lactones, and the nature of the catalyst/initiator system is different from other 'living' polymerization approaches. The initiation step for cyclic monomers contains the coordination of a monomer to a metal catalyst (usually late transition metals) and subsequently insertion ring-opening polymerization of monomers, which can effectively control the polymers features such as molecular weight and the dispersity [37, 38].

The objective of the present work was to covalent functionalization of graphene oxide (GO) with poly(2-hydroxyethyl methacrylate)-*graft*-poly(ε-caprolactone) [P(HEMA-*g*-CL)] via 'living' polymerization techniques and preparation of its electrospun nanofibers with gelatin. For this purpose, the GO was synthesized by oxidizing pristine graphite powder and then acetyl chloride was incorporated into the GO to produce an ATRP macroinitiator. The PHEMA was grafted onto GO in the presence of $N,N,N',N'',N''$-pentamethyldiethylenetriamine (PMDETA)/copper(I) chloride (CuCl) catalyst system via ATRP technique. Afterward, CL was graft copolymerized from hydroxyl groups of the PHEMA via ROP method to afford GO-*g*-[P(HEMA-*g*-CL)] nanocomposite. Finally, solutions of the GO-*g*-[P(HEMA-*g*-CL)] and gelatin were electrospun to produce uniform, conductive, and biocompatible nanofibers.

# 2 Experimental

## 2.1 Materials

Graphite, potassium permanganate ($KMnO_4$), sodium nitrate ($NaNO_3$), hydrochloric acid (HCl), sulfuric acid ($H_2SO_4$), $N,N,N',N'',N''$-pentamethyldiethylenetriamine (PMDETA), triethylamine (TEA), chloroacetyl chloride, and tin octanoate [$Sn(Oct)_2$] were purchased from Merck (Darmstadt, Germany) and were used as received. The monomers 2-hydroxyethyl methacrylate (HEMA) and ε-caprolactone (ε-CL) were purchased from Merck, dried over calcium hydride ($CaH_2$), distilled under reduced pressure, and then stored at −20 °C prior to use. Copper(I) chloride (CuCl; Merck) was purified by stirring in glacial acetic acid for about 1 h, then washing with methanol, and finally dried in vacuum oven at room temperature. All other chemicals and solvents were of analytical grade (Sigma-Aldrich) and purified according to standard methods.

## 2.2 Synthesis of GO from graphite

The GO was synthesized using modified Hummers' method as follows. Briefly, a 500-ml three-necked round-bottom flask was charged with $NaNO_3$ (3.0 g, 35 mmol), graphite powder (6.0 g), and $H_2SO_4$ (95–98%; 360 ml). The reaction mixture was stirred for about 20 min at room temperature, and then, $KMnO_4$ (18.0 g, 114 mmol) was slowly added into the reaction mixture, while the temperature remains under 20 °C. At the end of this period, temperature was increased to 35 °C, and the reaction mixture was stirred for about 7 h. Afterward, $KMnO_4$ (18.0 g, 114 mmol) was added into the flask and stirring continued for another 12 h at 35 °C. The reaction mixture was diluted by 1000 ml deionized water, and then, 60 ml of $H_2O_2$ (30 wt%) was added into the diluted product to reduce the unreacted $KMnO_4$. The crude product was centrifuged and washed with hydrochloric acid (HCl) solution (1 moll$^{-1}$) several times. The synthesized graphite oxide was washed with distilled water till its pH reached about 7. Finally, the graphite oxide dispersion (0.1 mg ml$^{-1}$) was exfoliated by sonication for about 1 h. The suspension was centrifuged, and the GO powder was obtained after drying in reduced pressure at 60 °C [39, 40].

## 2.3 Synthesis of acetyl chloride-functionalized graphene oxide (GO-Cl)

The synthesized GO (1.0 g) was added to 50 ml of dried $N,N$-dimethylformamide (DMF) and the mixture sonicated for 20 min in order to create a homogeneous dispersion. The suspension was transferred to a 100-ml three-necked

round-bottom flask, added TEA (2 ml; 14.4 mmol), and joined to the argon gas line. The reaction mixture was de-aerated by bubbling highly pure argon for 10 min and then added 1.1 ml (13.6 mmol) of chloroacetyl chloride under argon protection. The reaction mixture was stirred at room temperature under argon protection for about 24 h. At the end of this period, the content of the flask was centrifuged, washed with double-distilled water several times, and dried in reduced pressure at room temperature.

## 2.4  Synthesis of GO-*g*-PHEMA via ATRP technique

In a typical experiment, the GO-Cl (0.30 g) was dispersed in 20 ml dimethylsulfoxide (DMSO) through the sonication for about 20 min in order to create a homogeneous dispersion. The suspension was transferred to a 50-ml three-necked round-bottom flask charged with HEMA monomer (10 ml; 82.2 mmol), PMDETA (7 μl; 5 μmol), and CuCl (7 mg, 0.7 mmol). The reaction mixture was de-aerated for about 15 min and then stirred at room temperature under argon protection for about 72 h. At the end of this time, the crude product was diluted with DMSO (30 ml) and centrifuged (5000 rpm, 15 min) in order to remove copper complex. The suspension was poured in 300 ml of cold methanol, and then, the GO-*g*-PHEMA was obtained after filtering and drying.

## 2.5  Synthesis of GO-*g*-[P(HEMA-*g*-CL)] via ROP technique

The synthesized GO-*g*-PHEMA (0.5 g) was suspended in dried DMF (20 ml) by sonication for about 20 min. The suspension was transferred to a 50-ml three-necked round-bottom flask equipped with a condenser, gas inlet/outlet, and a magnetic stirrer. The monomer (CL; 7.8 ml, 70 mmol) and tin octanoate (0.05 g, 0.10 mmol) were added to the flask. The reaction mixture was stirred and de-aerated by bubbling highly pure argon for 10 min, and then, the flask was placed in an oil bath at 120 ± 3 °C. The reaction mixture was stirred at this temperature for about 24 h under inert atmosphere. At the end of this time, the crude product was cooled and diluted with $CH_2Cl_2$ (50 ml). The suspension was precipitated in a large amount of methanol. The product was filtered and dried in reduced pressure at room temperature.

## 2.6  Electrospinning of the GO-*g*-[P(HEMA-*g*-CL)] with gelatin

The GO-*g*-[P(HEMA-*g*-CL)]/gelatin nanofibers were fabricated by employing an electrospinning apparatus equipped with a high voltage power supply (Gamma High Voltage Research E8-50P, Ormond Beach, FL, USA).

Briefly, GO-*g*-[P(HEMA-*g*-CL)] (0.2 g) was dissolved in DMSO (10 ml) under ultrasound for about 1 h. In a separate container, 0.3 g of gelatin was dissolved in the same solvent (10 ml) at 50 °C. Thus, the concentrations of the GO-*g*-[P(HEMA-*g*-CL)] nanocomposite and gelatin solutions were 2 and 3% (w/v), respectively. Samples for electrospinning were then prepared by mixing two solutions together at volume ratio of GO-*g*-[P(HEMA-*g*-CL)] to gelatin at 30:70. The polymer solution was placed in a 10-ml syringe with a 23G hypodermic stainless steel needle used as the nozzle. The flow rate of the polymer solution was controlled with a precision pump (JZB 1800D double channel syringe pump, China) to feed at a constant rate. The flow rate of feed solution was fixed as 0.5 ml h$^{-1}$, and the applied voltage was set to 20 kV. The static collector was wrapped with aluminum foil, and the tip-to-collector distance was fixed at 15 cm. The fiber mats were dried overnight in reduced pressure at 30 °C.

## 2.7  Cell culture

The human osteoblast MG-63 cells were obtained from Iranian National Cell Bank (Pasteur Institute, Tehran, Iran) and cultivated in RPMI1640 having 100 IU penicillin per 100 mg streptomycin, enriched with 10% (v/v) of fetal bovine serum (FBS; Invitrogen, Carlsbad, CA, USA). The cells were cultured into flasks and kept in a humidified incubator with 5% $CO_2$ at 37 °C, and the media were refreshed twice weekly.

## 2.8  *In vitro* cytotoxicity assay

The standard colorimetric assay based on tetrazolium dye, 3-(4,5-dimethylthiazol-2-yl)-2,5-diphenyltetrazolium bromide (MTT), bio-reduction was performed for evaluation the cytotoxic effects of the fabricated nanofibers. Briefly, 96-well plates were coated well with sterilized (using gamma radiation) GO-*g*-[P(HEMA-*g*-CL)]/gelatin nanofibers; then, the human osteoblast MG-63 cells were seeded and incubated for 48 h. At the end of this time, the media were removed and 50 μl of MTT solution was added to each well followed by 150 μl cultivation medium, then placed in a cell culture incubator for 4 h. Finally, the remaining MTT solution aspirated, the formed formazan crystals were dissolved in DMSO, and absorbance was measured at 570 nm using a spectrophotometric plate reader, ELx 800 (Biotek, San Francisco, CA, USA) [59].

## 2.9  Characterization

Fourier transform infrared (FTIR) spectra of the samples were recorded on a Shimadzu 8101 M FTIR (Shimadzu, Kyoto, Japan) in the wave numbers range of

4000–400 cm$^{-1}$ with a resolution of 4 cm$^{-1}$. For sample preparation, the dry powders were grounded with potassium bromide (KBr) and compressed the mixture into disks. Ultraviolet–visible (UV–vis) spectra were recorded with a Shimadzu 1650 PC UV–vis spectrophotometer (Shimadzu, Kyoto, Japan) in the wavelength range of 600–200 nm. The thermal properties of the synthesized samples were investigated by means of thermogravimetric analyzer (TGA-PL STA 1640 equipment (Polymer Laboratories, Shropshire, UK)). The TGA experiments were conducted under a nitrogen atmosphere from 25–700 °C with heating rate of 10 °C min$^{-1}$. The morphologies of the synthesized samples were studied using field emission scanning electron microscope (FE-SEM) type 1430 VP (LEO Electron Microscopy Ltd, Cambridge, UK). Atomic force microscopy (AFM; JPK Instruments AG, Berlin, Germany) images were recorded in non-contact tapping mode. X-ray diffraction (XRD) patterns were obtained with Siemens D5000 (Aubrey, Texas, USA), X-ray generator (CuK$_\alpha$ radiation with $\lambda = 1.5406$ Å) with a $2\theta$ scan range of 2–40° at room temperature. The wettability of the electrospun nanofibers was studied by water drop contact angle measurement using OCA 20 Plus contact angle meter system (DataPhysics Instruments GmbH, Filderstadt, Germany). The droplet size was 5 µl, and at least five samples were used for each test. The conductivities of the synthesized samples were measured using the standard four-probe technique (Azar Electrode, Urmia, Iran) at room temperature.

# 3 Results and discussion

A relatively novel achievement with graphene and its derivatives (especially graphene oxide) is their application in the fabrication of high-performance and functional nanofiber scaffolds, in part due to their unique electrical conductivity and biological properties [41–44]. In the field of regenerative medicine, the incorporation of electrically conductive materials (e.g., graphene) into the scaffold can provide a physical conductive substrate for the local delivery of an electrical stimuli to a specific site to foster cell growth and repair damaged tissue [45, 46]. As mentioned, the aim of this study is the covalent functionalization of graphene oxide (GO) with poly(2-hydroxyethyl methacrylate)-*graft*-poly(ε-caprolactone) [P(HEMA-*g*-CL)] via 'living' polymerization techniques and preparation of its electrospun nanofibers with gelatin. The overall methodologies are shown in Schemes 1, 2, and 3. The prepared electrospun nanofibers may be considered as suitable materials having proper conductivity, biocompatibility, and hydrophilicity for tissue engineering applications.

## 3.1 Characterization of GO

The X-ray pattern and UV–vis spectrum of the synthesized GO are shown in Fig. 1. As seen in X-ray pattern, the sharp diffraction peak observed at $2\theta = 10.68°$ with an interlayer distance of 0.84 nm corresponds to GO nanosheets. The UV–vis spectrum of GO shows maximum absorption peaks at 237 and 303 nm attributable to π–π* and n–π* transitions of aromatic C=C bonds, respectively. These XRD and UV–vis analysis assignments verify that the GO was successfully synthesized from graphite.
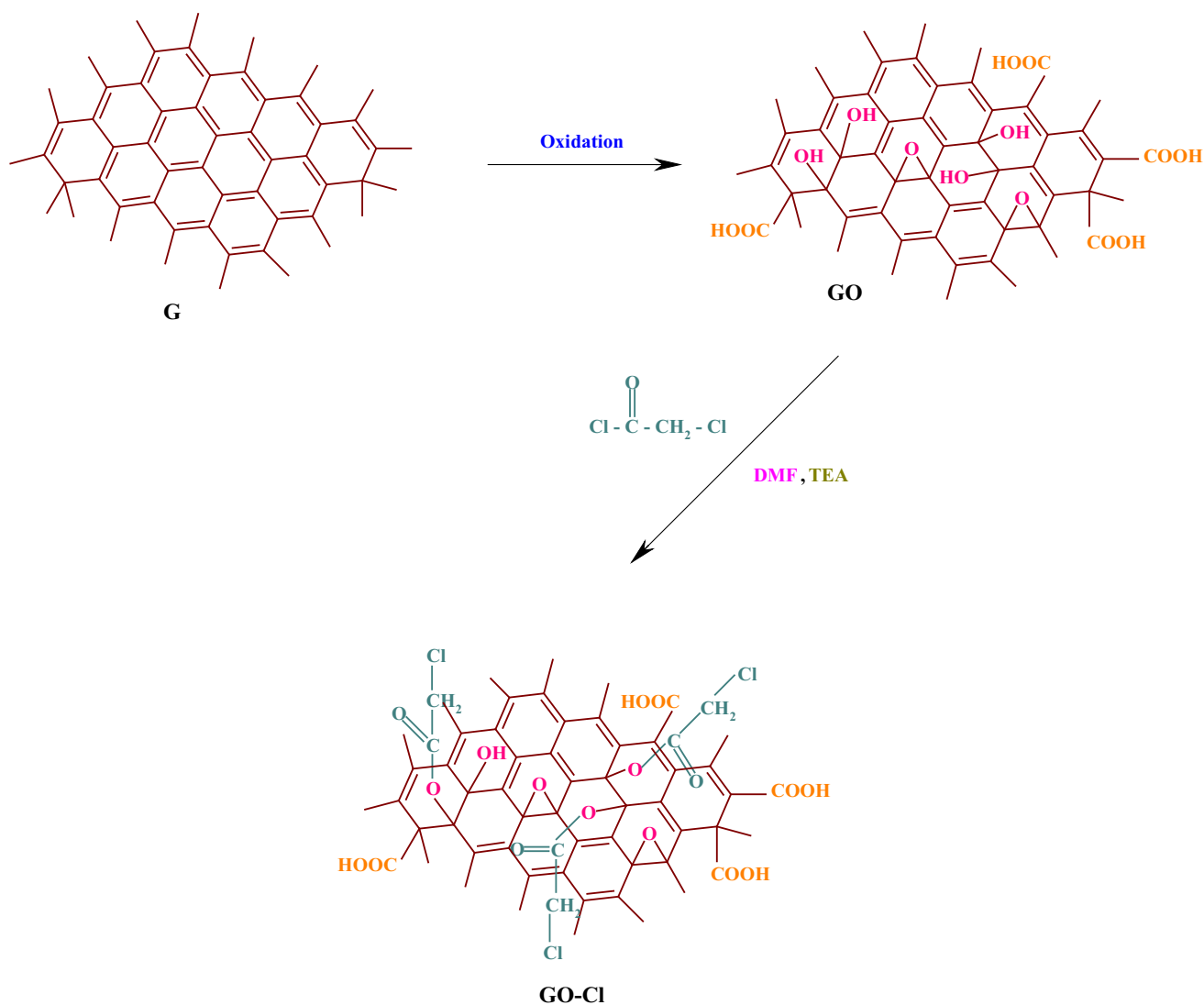
## 3.2 Synthesis of GO-Cl

Figure 2 depicts the FTIR spectra of graphite, GO, and GO-Cl samples. As shown in figure, the graphite only shows a weak band at 1481 cm$^{-1}$ corresponding to the stretching vibration of aromatic C=C. In contrast, the GO shows the characteristic absorption bands attributable to the carbonyl stretching vibration at 1728 cm$^{-1}$, stretching vibrations of C–O groups of the epoxy, and carboxylic acid at 1204 and 1197 cm$^{-1}$, respectively, and C–O–C stretching vibration at 1047 cm$^{-1}$. In addition, the hydroxyl groups were observed as a broad strong band centered at 3364 cm$^{-1}$. After incorporation of the acetyl chloride group into the GO, the most significant changes in the FTIR spectrum of the GO-Cl are the appearance of stretching vibrations of aliphatic and aromatic C–H at 3050–2850 cm$^{-1}$ region, and C–Cl stretching vibration at 654 cm$^{-1}$. Furthermore, as seen in this spectrum, the intensity of the hydroxyl stretching vibration is decreased significantly. This verifies that most of the hydroxyl groups were converted to acetyl chloride groups.

## 3.3 Synthesis of GO-*g*-[P(HEMA-*g*-CL)]

It is well established that the PCL is semicrystalline, easily obtainable, non-toxic, biocompatible, and biodegradable synthetic aliphatic polyester. PCL is considered as a soft- and hard-tissue-compatible synthetic biopolymer. Despite, PCL has low cellular affinity due to its crystallinity and hydrophobicity. Some procedures such as synthesis of its copolymers with hydrophilic polymers, co-electrospinning of PCL with different biopolymers or nanoparticles, and post-electrospinning modifications have been adapted to overcome these problems [47, 48]. The hydrophilicity and biological activity of PCL have been significantly improved by a combination of natural biopolymers, such as collagen [49], chitosan [50], and gelatin [51].

The FTIR spectra of the GO-*g*-PHEMA and GO-*g*-[P(HEMA-*g*-CL)] samples are shown in Fig. 3. The FTIR spectrum of the GO-*g*-PHEMA shows the characteristic absorption bands due to the stretching vibration of carbonyl
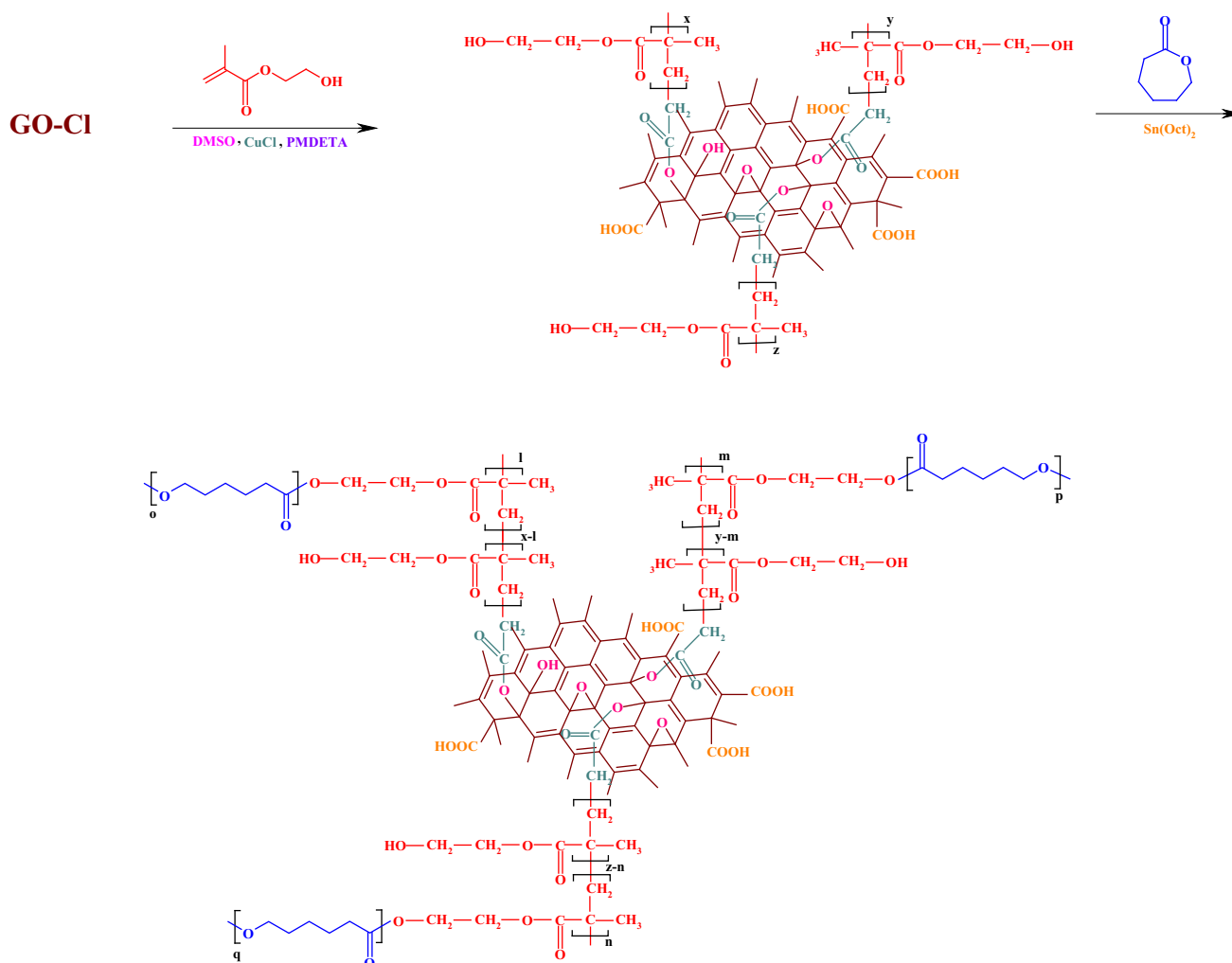
**Scheme 1** Synthesis of GO and GO-Cl

group at 1722 cm$^{-1}$, C–H bending vibrations at 1466 cm$^{-1}$, stretching vibration of C–O group at 1372, and C–O–C stretching vibration at 1117 cm$^{-1}$. The broad strong band centered at 3368 cm$^{-1}$ is related to the hydroxyl group of the PHEMA. It should be pointed out that the stretching vibrations of aliphatic C–H are overlapped with the hydroxyl broad and strong band. After grafting of PCL onto GO-*g*-PHEMA, the most significant changes in the FTIR spectrum are the decreasing of the stretching vibration of hydroxyl group and appearance of C–H stretching vibrations at 3000–2800 cm$^{-1}$ region.

### 3.4 Thermal property study

As shown in Fig. 4, the thermal properties of graphite, GO, GO-Cl, GO-*g*-PHEMA, and GO-*g*-[P(HEMA-*g*-CL)] were investigated by means of thermogravimetric analysis

(TGA) under nitrogen flow. According to the results, the pristine graphite is almost stable till 500 °C, and the residue at 650 °C for pristine graphite is about 95 wt%. As mentioned previously, due to reactive oxygen functional groups (*e.g.,* epoxide, hydroxyl, and carboxyl groups), the GO has strong hydrophilic property; thus, water molecules may be adsorbed in stacked structure of GO. Consequently, some mass loss around 100 °C is observed for GO. In addition, the TGA curve of the GO exhibits a two-step weight loss process; the first step (120–220 °C) corresponds to the CO, CO$_2$, and steam release from the most labile functional groups, whereas the second step (220–310 °C) is associated with the degradation of more stable oxygen functionalities. After which the loss rate slows down, and the residue at 650 °C for GO is 38 wt%. It should be pointed out that the weight loss between 310 and 650 °C is related to the pyrolysis of the carbon skeleton.

**Scheme 2** Synthesis of GO-*g*-PHEMA and GO-*g*-[P(HEMA-*g*-CL)]

The TGA thermogram of the GO-Cl shows similar degradation process with minor differences. The most distinctive future in this thermogram is the acceleration of weight loss between 120 and 250 °C, mainly due to the degradation of acetyl chloride moiety. The residue at 650 °C for GO-Cl is about 41 wt%.

In contrast, the TGA curve of the GO-*g*-PHEMA shows the major weight loss around 250–380 °C. The initial weight loss (~8 wt%) up to 250 °C is related to the CO, $CO_2$, and steam release from GO. The residue at 650 °C for GO-*g*-PHEMA is about 19 wt%. The TGA thermogram of the GO-*g*-[P(HEMA-*g*-CL)] exhibits the major degradation around 300–650 °C. The initial weight loss (~9 wt%) up to 250 °C is related to the CO, $CO_2$, and steam release from GO or evaporation of any solvent. The residue at 650 °C for GO-*g*-[P(HEMA-*g*-CL)] is about 11 wt%.

## 3.5 Morphology analysis

The surface morphologies of the GO-*g*-PHEMA and GO-*g*-[P(HEMA-*g*-CL)] nanocomposites were observed by means of FE-SEM and AFM as shown in Figs. 5 and 6. The FE-SEM images of both samples (Fig. 5) showed that the polymer chains grew from GO nanosheets, and this resulted to wrinkled and folded morphologies in both samples. In addition, it is also clear that in both samples polymeric chains [PHEMA and P(HEMA-*g*-CL)] were covered the surfaces of the nanosheets, and the graphene oxide nanosheets were dispersed well in the polymeric matrix.

Figure 6 shows the two- and three-dimensional AFM topography images for the GO-*g*-PHEMA (top) and GO-*g*-[P(HEMA-*g*-CL)] (bottom) samples. The dark regions represent valleys, and the brightest regions show the

**Scheme 3** Overall strategy for the fabrication of biocompatible, porous, and electrically conductive GO-*g*-[P(HEMA-*g*-CL)] electrospun nanofibers
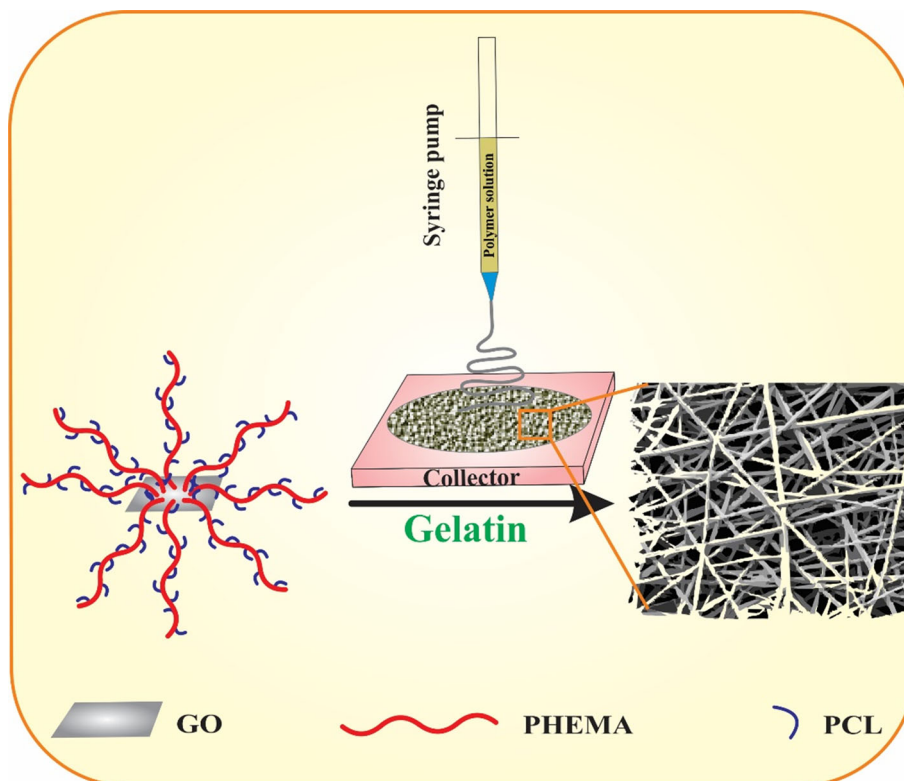


**Fig. 1** X-ray pattern (*left*) and UV–vis spectrum (*right*) of the GO
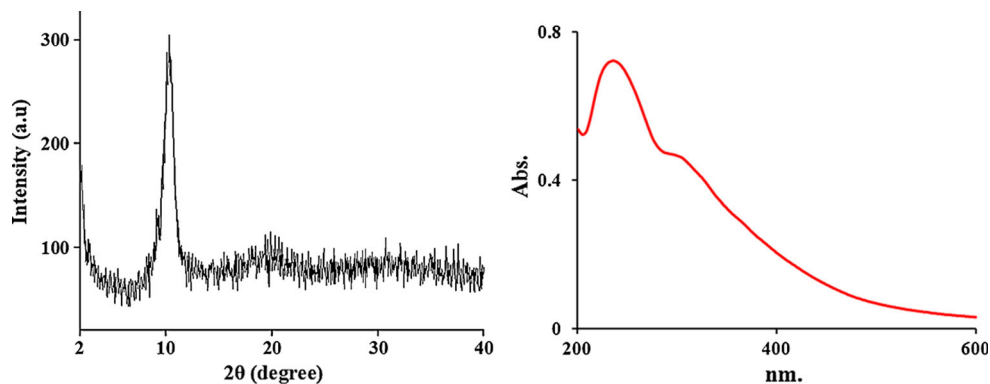


highest point of the nanocomposites. The three-dimensional AFM topography images exhibited the surfaces of both samples are relatively rough with some protuberances, mainly due to growth of PHEMA and P(HEMA-*g*-CL) chains onto the functionalized GO.

## 3.6 Characterization of GO-*g*-[P(HEMA-*g*-CL)]/ gelatin electrospun nanofibers

### 3.6.1 Morphology study

Various approaches such as solvent casting/particle leaching [52], thermally induced phase separation (TIPS) [53], gas foaming [54], rapid prototyping (additive manufacturing) [55], and electrospinning [56] have been developed or introduced for scaffold fabrication. Among them, electrospinning is an efficient and simple approach that can be tuned for fabrication of fibers with a diameter ranging from tens of nanometers to a few microns. Electrospun polymeric nanofibrous possess a large surface area-to-volume ratio, high porosity, flexibility in design of surface functionalities, and superior mechanical properties. These nanofibers are considered as promising materials for a wide variety of applications, such as drug delivery, optoelectronics, sensor technology, as well as regenerative medicine [48, 57–60].
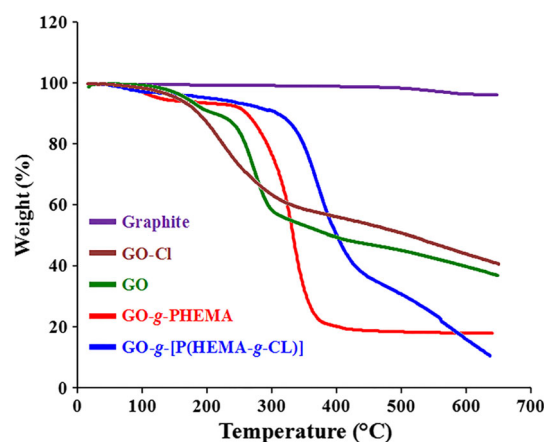
The surface morphologies of the GO-*g*-[P(HEMA-*g*-CL)]/gelatin electrospun nanofibers were studied by means of FE-SEM (Fig. 7). As seen, the three-dimensional interconnected pore structure with average diameters in the size
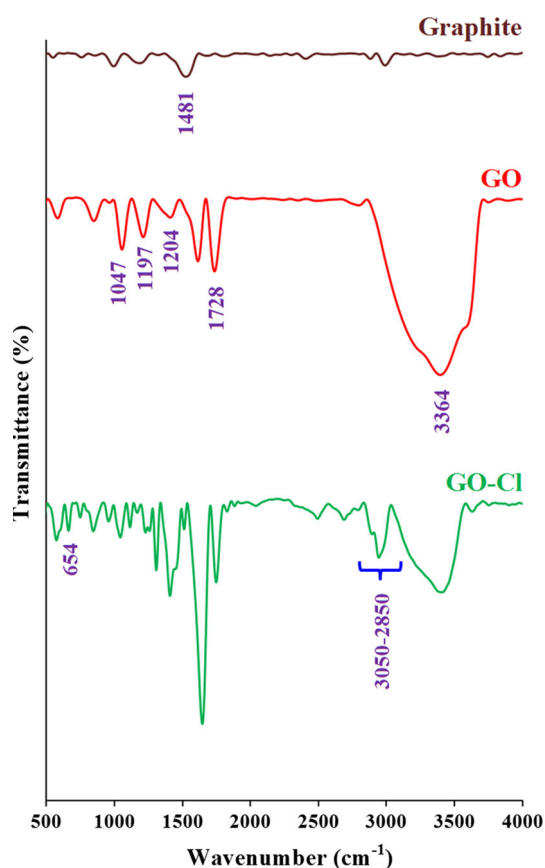
**Fig. 2** FTIR spectra of graphite, GO, and GO-Cl
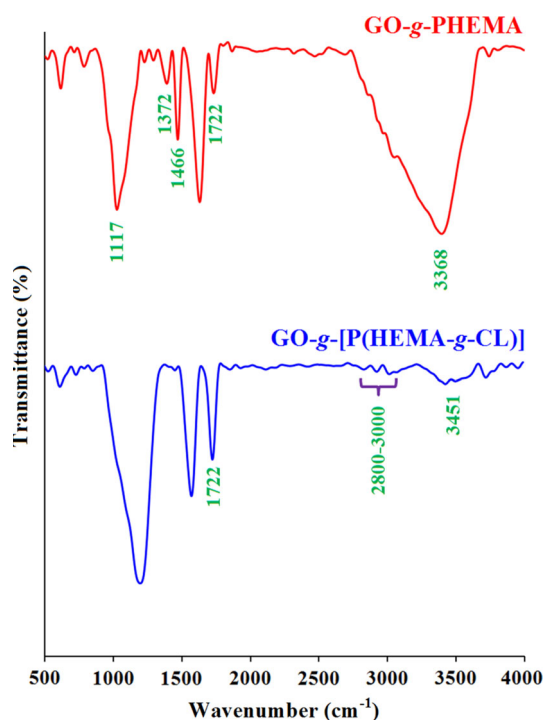


**Fig. 3** FTIR spectra of GO-*g*-PHEMA and GO-*g*-[P(HEMA-*g*-CL)]



**Fig. 4** TGA curves of graphite, GO, GO-Cl, GO-*g*-PHEMA, and GO-*g*-[P(HEMA-*g*-CL)]

range of $100 \pm 40$ nm was formed for electrospun nanofibers. In addition, as seen in FE-SEM image, some of the electrospun nanofibers were fractured and disconnected.

### 3.6.2 Biodegradability and hydrophilicity

Biodegradable implantable polymeric scaffolds have the advantage of avoiding a chronic inflammation due to their long stay in the body, as well as avoiding subsequent surgical removal. Hence, in vivo evaluation of biodegradability of biomaterials is a pivotal aspect in tissue engineering research. Among the various polymeric scaffolds, the PCL, PHEMA, and gelatin are promising candidates, mainly due to their biodegradabilities and biocompatibilites. In addition, PHEMA and gelatin have good hydrophilicities. As cells develop and lay down the extracellular matrix (ECM), the scaffold should begin to degrade. The rate of degradation can be affected by the macroscopic shape and the timely tissue integration [48, 59–61].

The GO-*g*-[P(HEMA-*g*-CL)]/gelatin electrospun nanofibers were cross-linked in glutaraldehyde vapor (sample was put on the tops of 50 wt% glutaraldehyde aqueous solution (20 ml) in closed glass desiccator) for about 4 h at room temperature. Afterward, the in vitro degradability of the GO-*g*-[P(HEMA-*g*-CL)]/gelatin electrospun nanofibers was studied through evaluating the morphological changes and gravimetric measurements after soaking the nanofibers in phosphate-buffered saline (PBS; pH 7.4; Invitrogen, CA, USA) at 37 °C. The PBS was refreshed every five days. After reaching the designed time, the specimens were retrieved, washed several times with double-distilled water, dried in vacuum, and then weighted. The mass loss percentage was calculated from: $(W_i–W_r)/W_i$; where $W_i$ and $W_r$ are the initial and the residual dry weights of the electrospun nanofibers. After 10 days, the mass loss for the GO-*g*-
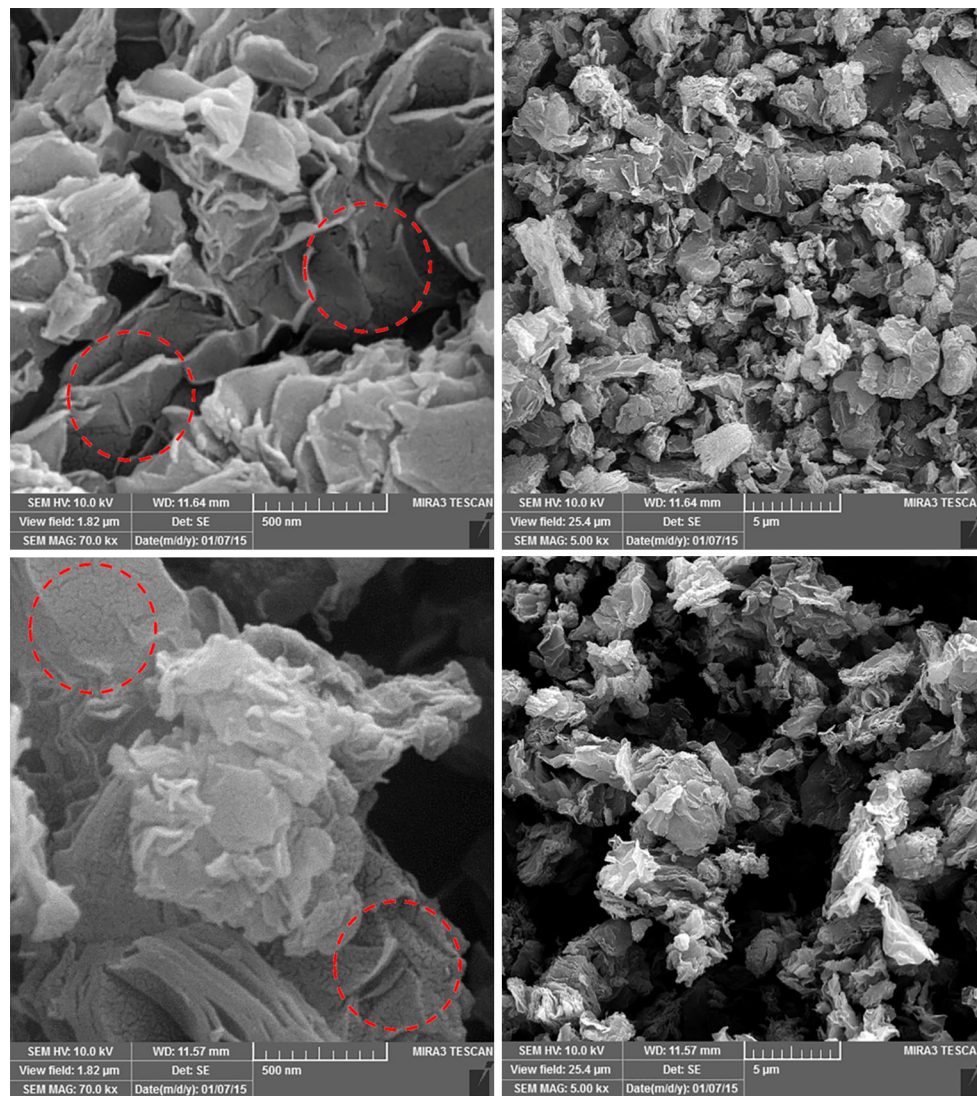
**Fig. 5** FE-SEM images of GO-*g*-PHEMA (*top*) and GO-*g*-[P(HEMA-*g*-CL)] (*bottom*) at different magnifications

[P(HEMA-*g*-CL)]/gelatin electrospun nanofibers was calculated to be 18 wt%.

The in vitro degradability of the electrospun nanofibers was further verified by evaluating the morphological changes after soaking the nanofibers in PBS at 37 °C. Figure 8 (right) shows the FE-SEM image of the nanofibers after 10-day soaking in PBS. As shown in figure, the electrospun nanofibers undergo swelling and degradation after 10 days.

It should be pointed out that the protein and inducer adsorption and cell attachment significantly affected by hydrophilicity of the scaffold. The ideal hydrophilicity depends on the different cell types and surface modification techniques [62]. The water drop contact angle of the GO-*g*-[P(HEMA-*g*-CL)]/gelatin electrospun nanofibers was measured at room temperature to investigate the surface hydrophilicity of the nanofibers. The contact angle of the electrospun nanofibers with water was calculated to be $76 \pm 2.2°$. Furthermore, the photographs of water drop on GO-*g*-[P(HEMA-*g*-CL)]/gelatin electrospun nanofibers are shown in Fig. 8 (left).

### 3.7 Electrical conductivity measurement

The electrical conductivities of the samples were measured by the standard four-probe technique at room temperature. The experimental determinations were repeated five times for each sample to assess the sample accuracy. Furthermore, the conductivities were preserved for at least 100 h post-fabrication. The electrical conductivities ($\sigma$; S cm$^{-1}$) of the samples were calculated using the following equations:
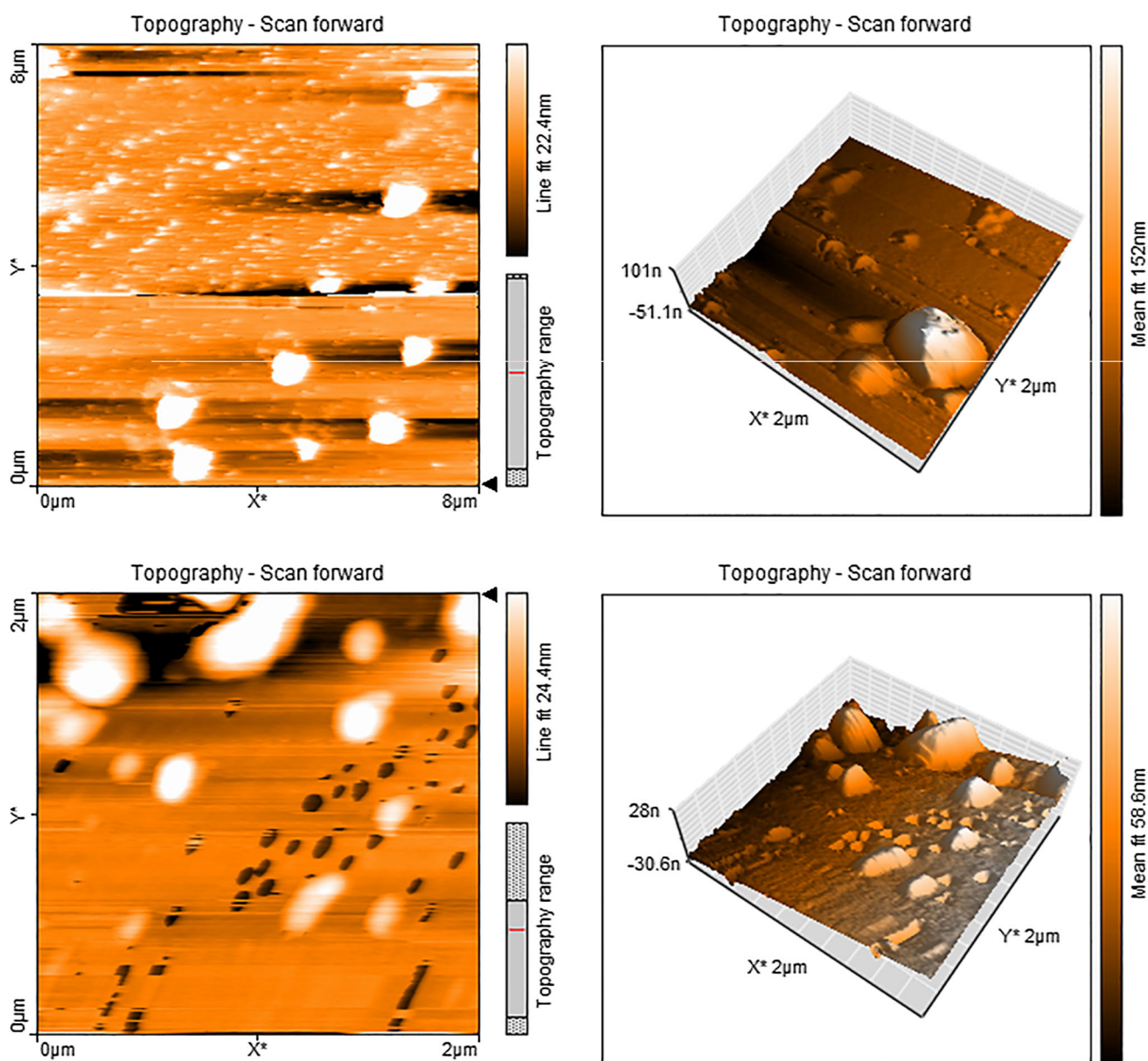
**Fig. 6** Two-dimensional (*left*) and three-dimensional (*right*) AFM topography images of GO-*g*-PHEMA (*top*) and GO-*g*-[P(HEMA-*g*-CL)] (*bottom*)

$$\rho = (V/I)\,(\pi/\ln 2)\mathrm{d}$$

$$\sigma = 1/\rho$$

where $V$ is voltage, $I$ is current passed through outer probes, d is thicknesses of the sample, and $\rho$ ($\Omega$ cm) is volume-specific resistivity.

The electrical conductivity results obtained are summarized in Table 1. As shown in table, the electrical conductivity of the GO after functionalization with PHEMA and PHEMA-*g*-PCL was decreased continually, because both PHEMA and PCL are non-conductive materials. Moreover, as expected after electrospinning, the electrical

conductivity of the GO-*g*-[P(HEMA-*g*-CL)]/gelatin electrospun nanofibers decreased significantly in comparison with GO-*g*-[P(HEMA-*g*-CL)] sample, since gelatin is an insulating material. However, the conductivity in the semiconductor range ($\sim 10^{-5}$ S cm$^{-1}$) is sufficient for regenerative medicine purpose [63, 64].
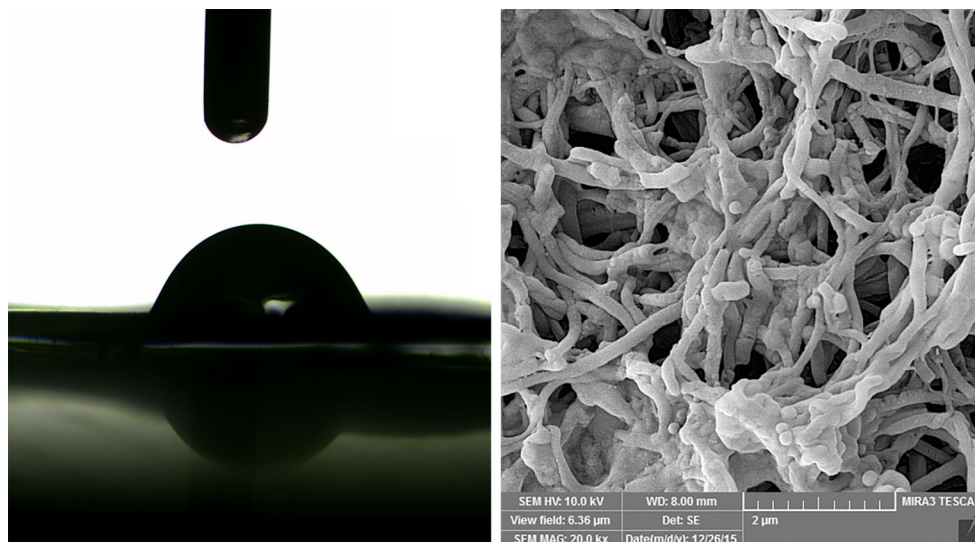
### 3.8 Biocompatibility

The biocompatibility of any material is the first and pivotal requirement for scaffolding, mainly due to its direct influence on cells attachment, proliferation, migration,
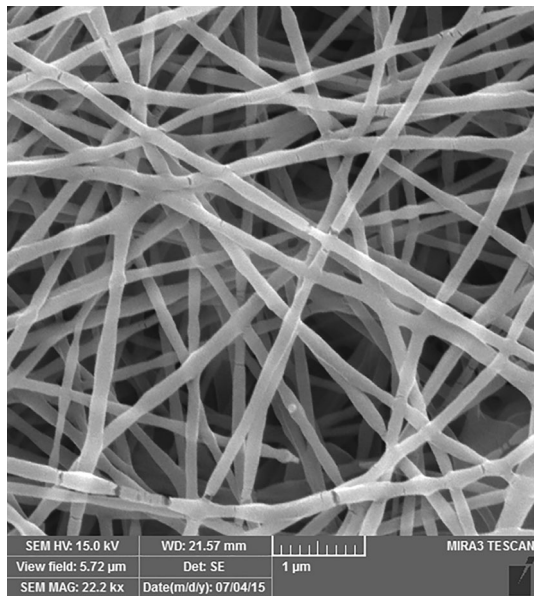
**Fig. 7** FE-SEM image of GO-*g*-[P(HEMA-*g*-CL)]/gelatin electrospun nanofibers

differentiation, and *neo*-tissue formation. In this respect, PCL, PHEMA, and gelatin can be considered as biocompatible materials that qualified them for a wide variety of biomedical applications [59, 65, 66]. The biocompatibility of the fabricated scaffold was evaluated by MTT assay, and the results obtained are summarized in Fig. 9. As shown in figure, in comparison with negative control (polystyrenic well plates), the fabricated scaffold did not able to induce cytotoxicity in human osteoblast MG-63 cells.

**Table 1** Electrical properties of the samples

| Sample | Volume-specific resistivity ($\rho$; $\Omega$ cm) | Electrical conductivity ($\sigma$; S cm$^{-1}$) |
|---|---|---|
| GO | 0.58 | 1.72 |
| GO-*g*-PHEMA | 2.94 | 0.34 |
| GO-*g*-[P(HEMA-*g*-PCL)] | 125 | 0.008 |
| GO-*g*-[P(HEMA-*g*-PCL)]/gelatin[a] | 54,644 | $1.83 \times 10^{-5}$ |

[a] The electrospun nanofibers were provided as mentioned in Experimental section

## 4 Conclusion

Taking together, this study has shown a convenient, simple, and powerful approach to preparation of GO-*g*-[P(HEMA-*g*-CL)]/gelatin electrospun nanofibers for potential application in regenerative medicine, mainly due to its electrical conductivity, biocompatibility, biodegradability, and versatile materials morphology. The chemical structures of all samples as representatives were characterized by means of FTIR spectroscopy. The electrical conductivity of the fabricated GO-*g*-[P(HEMA-*g*-CL)]/gelatin electrospun nanofibers was obtained to be $1.83 \times 10^{-5}$ which represents proper conductivity for scaffolding. The FE-SEM image showed that the nanofibers were formed in three-dimensional interconnected pore structure, with average diameters in the size range of $100 \pm 40$ nm. The biocompatibility of the fabricated electrospun nanofibers was confirmed through the assessing survival rate of human osteoblast MG-63 cells on nanofibers using the MTT assay.



**Fig. 8** Photographs of water drop on GO-*g*-[P(HEMA-*g*-CL)]/gelatin electrospun nanofibers (*left*) and the FE-SEM image of the GO-*g*-[P(HEMA-*g*-CL)]/gelatin electrospun nanofibers after 10-day soaking in PBS
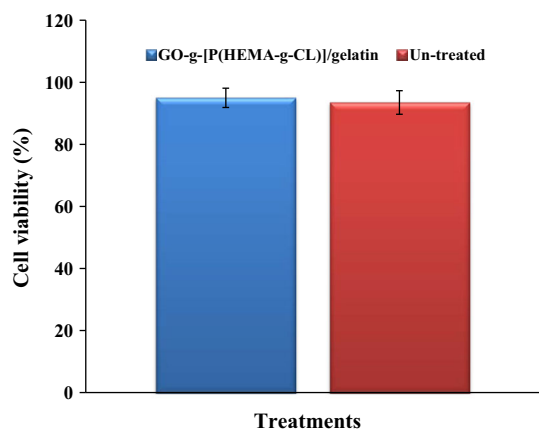
**Fig. 9** *In vitro* cytotoxic effects of the GO-*g*-[P(HEMA-*g*-CL)]/gelatin electrospun nanofibers on human osteoblast MG-63 cells

The in vitro degradability of the nanofibers was studied through evaluating the morphological changes and gravimetric measurements. These assays exhibited suitable degradability for the fabricated nanofibers. It would be expected that electrically conductive scaffolds will be further developed in the coming decades. In conclusion, further experiments are under progress in order to investigate the effect of composition, conductivity, and other physicochemical properties in performance of the fabricated GO-*g*-[P(HEMA-*g*-CL)]/gelatin electrospun nanofibers in adhesion, proliferation, migration, and differentiation of various cell lines.

# References

1. M. Xiao, T. Kong, W. Wang, Q. Song, D. Zhang, Q. Ma, G. Cheng, Adv. Funct. Mater. **25**, 6165 (2015)
2. M.Y. Lim, H. Shin, D.M. Shin, S.S. Lee, J.C. Lee, Polymer **84**, 89 (2016)
3. M.M. Tavakoli, A. Simchi, Z. Fan, H. Aashuri, Chem. Commun. **52**, 323 (2015)
4. M. Faraji, Appl. Phys. A **122**, 697 (2016)
5. A. Noparvar-Qarebagh, H. Roghani-Mamaqani, M. Salami-Kalajahi, Polym. Degrad. Stabl. **124**, 1 (2016)
6. H. Shen, L. Zhang, M. Liu, Z. Zhang, Theranostics **2**, 283 (2012)
7. F. Sarhadi, M.S. Afarani, D. Mohebbi-Kalhori, M. Shayesteh, Appl. Phys. A **122**, 390 (2016)
8. A.K. Geim, Science **324**, 1530 (2009)
9. A.K. Geim, K. Novoselov, Nat. Mater. **6**, 183 (2007)
10. X.S. Li, W.W. Cai, J.H. An, S. Kim, J. Nah, D.X. Yang, R. Piner, A. Velamakanni, I. Jung, E. Tutuc, S.K. Banerjee, L. Colombo, R.S. Ruoff, Science **324**, 1312 (2009)
11. K.S. Kim, Y. Zhao, H. Jang, S.Y. Lee, J.M. Kim, K.S. Kim, J.H. Ahn, P. Kim, J.Y. Choi, B.H. Hong, Nature **457**, 706 (2009)
12. M. Choucair, P. Thordarson, J.A. Stride, Nat. Nanotechnol. **4**, 30 (2009)
13. J. Wang, K.K. Manga, Q. Bao, K.P. Loh, J. Am. Chem. Soc. **133**, 8888 (2011)
14. S. Makharza, G. Cirillo, A. Bachmatiuk, I. Ibrahim, N. Ioannides, B. Trzebicka, S. Hampel, M.H. Rummeli, J. Nanopart. Res. **15**, 2099 (2013)
15. H. Sun, L. Zhang, W. Xia, L. Chen, Z. Xu, W. Zhang, Appl. Phys. A **122**, 632 (2016)
16. M.S. Ramasamy, S.S. Mahapatra, J.W. Cho, J. Colloid Interface Sci. **455**, 63 (2015)
17. F. Samadaei, M. Salami-Kalajahi, H. Roghani-Mamaqani, M. Banaei, RSC Adv. **5**, 71835 (2015)
18. Q. Jing, W. Liu, Y. Pan, V.V. Silberschmidt, L. Li, Z.L. Dong, Mater. Design. **85**, 808 (2015)
19. Y. Pan, H. Bao, N.G. Sahoo, T. Wu, L. Li, Adv. Funct. Mater. **21**, 2754 (2011)
20. S.H. Lee, D.R. Dreyer, J. An, A. Velamakanni, R.D. Piner, S. Park, Y. Zhu, S.O. Kim, C.W. Bielawski, R.S. Ruoff, Macromol. Rapid Commun. **31**, 281 (2010)
21. Y. Sun, J. Zhou, Q. Cheng, D. Lin, Q. Jiang, A. Dong, Z. Liang, L. Deng, J. Appl. Polym. Sci. **133**, 43303 (2016)
22. L. Kan, Z. Xu, C. Gao, Macromolecules **44**, 444 (2011)
23. H.M. Hegab, A. ElMekawy, T.G. Barclay, A. Michelmore, L. Zou, C.P. Saint, M. Ginic-Markovic, ACS. Appl. Mater. Interfaces **7**, 18004 (2015)
24. Z. Liu, S. Zhu, Y. Li, Y. Li, P. Shi, Z. Huang, X. Huang, Polym. Chem. **6**, 311 (2015)
25. Z. Liu, G. Lu, Y. Li, Y. Li, X. Huang, RSC Adv. **4**, 60920 (2014)
26. E.X. Liang, M. Lu, Z.H. Hou, Y. Huang, B.H. He, G.X. Wang, L.C. Liu, H. Wu, M. Zhong, J. Appl. Polym. Sci. **133**, 42891 (2016)
27. M. Jaymand, Macromol. Res. **19**, 998 (2011)
28. M. Jaymand, Polym. J. **43**, 186 (2011)
29. S. Ghasemi Karaj-Abad, M. Abbasian, M. Jaymand, Carbohydr. Polym. **152**, 297 (2016)
30. G. Moad, Polym. Int. **64**, 15 (2015)
31. A. Ghamkhari, B. Massoumi, M. Jaymand, Design. Monomer. Polym. **20**, 190 (2017)
32. K. Matyjaszewski, N.V. Tsarevsky, J. Am. Chem. Soc. **136**, 6513 (2014)
33. Z. Xue, D. He, X. Xie, Polym. Chem. **6**, 1660 (2015)
34. M. Jaymand, M. Hatamzadeh, Y. Omidi, Prog. Polym. Sci. **47**, 26 (2015)
35. C.W. Bielawski, R.H. Grubbs, Prog. Polym. Sci. **32**, 1 (2007)
36. M.R. Buehmeiser, Chem. Rev. **109**, 303 (2009)
37. A.K. Diallo, X. Michel, S. Fouquay, G. Michaud, F. Simon, J.M. Brusson, J.F. Carpentier, S.M. Guillaume, Macromolecules **48**, 7453 (2015)
38. B.F. Strick, M. Delferro, F.M. Geiger, R.J. Thomson, ACS. Sus. Chem. Eng. **3**, 1278 (2015)
39. W.S. Hummers, R.E. Offeman, J. Am. Chem. Soc. **80**, 1339 (1958)
40. D.C. Marcano, D.V. Kosynkin, J.M. Berlin, A. Sinitskii, Z. Sun, A. Slesarev, L.B. Alemany, W. Lu, J.M. Tour, ASC Nano. **8**, 4806 (2010)
41. J. Song, H. Gao, G. Zhu, X. Cao, X. Shi, Y. Wang, Carbon **95**, 1039 (2015)
42. Z. Liu, J.T. Robinson, X. Sun, H. Dai, J. Am. Chem. Soc. **130**, 10876 (2008)
43. H. Chen, M.B. Müller, K.J. Gilmore, G.G. Wallace, D. Li, Adv. Mater. **20**, 3557 (2008)
44. X. Shi, H. Chang, S. Chen, C. Lai, A. Khademhosseini, H. Wu, Adv. Funct. Mater. **22**, 751 (2012)
45. M. Gu, Y. Liu, T. Chen, F. Du, X. Zhao, C. Xiong, Y. Zhou, Tissue Eng. B. **20**, 477 (2014)

46. D.H. Kim, S.M. Richardson-Burns, J.L. Hendricks, C. Sequera, D.C. Martin, Adv. Funct. Mater. **17**, 79 (2007)
47. K. Fujihara, M. Kotaki, S. Ramakrishna, Biomaterials **26**, 4139 (2005)
48. L. Ghasemi-Mobarakeh, M.P. Prabhakaran, M. Morshed, M.H. Nasr-Esfahani, S. Ramakrishna, Biomaterials **29**, 4532 (2008)
49. A.L. Yin, K.H. Zhang, M.J. McClure, C. Huang, J. Wu, J. Fang, X. Mo, G.L. Bowlin, S.S. Al-Deyab, M. El-Newehy, J. Biomed. Mater. Res. A. **101**, 1292 (2013)
50. Y. Wan, H. Wu, X. Cao, S. Dalai, Polym. Degrad. Stabil. **93**, 1736 (2008)
51. M.A. Alvarez-Perez, V. Guarino, V. Cirillo, L. Ambrosio, Biomacromolecules **11**, 2238 (2010)
52. A. Brown, S. Zaky, H.R. Jr, C. Sfeir, Acta Biomater. **11**, 543 (2015)
53. L. Li, J. Ge, L. Wang, B. Guo, P.X. Ma, J. Mater. Chem B. **2**, 6119 (2014)
54. W.W. Thein-Han, H.H.K. Xu, Tissue Eng. A. **19**, 1675 (2013)
55. S.H. Park, D.S. Park, J.W. Shin, Y.G. Kang, H.K. Kim, T.R. Yoon, J.W. Shin, J. Mater. Sci. Mater. Med. **23**, 2671 (2012)
56. T. Jiang, E.J. Carbone, K.W.H. Lo, C.T. Laurencin, Prog. Polym. Sci. **46**, 1 (2015)
57. K.I. Kwon, S. Kidoaki, T. Matsuda, Biomaterials **26**, 3929 (2005)
58. B. Massoumi, S. Davtalab, M. Jaymand, A.A. Entezami, RSC Adv. **5**, 36715 (2015)
59. R. Sarvari, B. Massoumi, M. Jaymand, Y. Beygi-Khosrowshahi, M. Abdollahi, RSC Adv. **6**, 19437 (2016)
60. B. Massoumi, N. Aalia, M. Jaymand, RSC Adv. **5**, 107680 (2015)
61. R. Cheng, X. Wang, W. Chen, F. Meng, C. Deng, H. Liu, Z. Zhong, J. Mater. Chem. **22**, 11730 (2012)
62. Q. Li, Z. Chang, G. Oliveira, M. Xiong, L.M. Smith, B.L. Frey, N.V. Welham, Biomaterials **81**, 104 (2016)
63. L. Huang, J. Hu, L. Lang, X. Wang, P. Zhang, X. Jing, X. Wang, X. Chen, P.I. Lelkes, A.G. MacDiarmid, Y. Wei, Biomaterials **28**, 1741 (2007)
64. T.H. Qazi, R. Rai, A.R. Boccaccini, Biomaterials **35**, 9068 (2014)
65. C.J. Bettinger, J.P. Bruggeman, A. Misra, J.T. Borenstein, R. Langer, Biomaterials **30**, 3050 (2009)
66. B. Massoumi, M. Ramezani, M. Jaymand, M. Ahmadinejad, J. Polym. Res. **22**, 214 (2015)